

# Characterization and functional role of voltage gated cation conductances in the glucagon-like peptide-1 secreting GLUTag cell line

F. Reimann<sup>1</sup>, M. Maziarz<sup>2</sup>, G. Flock<sup>2</sup>, A. M. Habib<sup>1</sup>, D. J. Drucker<sup>2</sup> and F. M. Gribble<sup>1</sup>

<sup>1</sup>Cambridge Institute for Medical Research, University of Cambridge, Department of Clinical Biochemistry, Wellcome Trust/MRC Building, Addenbrooke's Hospital, Hills Road, Cambridge CB2 2XY, UK

<sup>2</sup>Banting and Best Diabetes Centre, University of Toronto, Toronto General Hospital, 200 Elizabeth Street MBRW-4R402, Toronto, Canada M5G 2C4

Glucagon-like peptide-1 (GLP-1) is released from intestinal L-cells in response to nutrient ingestion. It is currently under therapeutic evaluation because it enhances insulin secretion in type 2 diabetes. Previous studies using the GLP-1 secreting cell line GLUTag have shown that the cells are electrically active, and that the action potential frequency is regulated by nutrients. In this study we characterize voltage gated currents underlying this electrical activity and correlate the electrophysiological findings with gene expression determined by microarrays. Whole cell voltage clamp experiments designed to separate different ionic components revealed rapidly inactivating sodium currents sensitive to tetrodotoxin, calcium currents sensitive to nifedipine and  $\omega$ -conotoxin GVIA, and sustained as well as rapidly inactivating potassium currents, which were sensitive to TEA and 4-AP, respectively. In perforated patch experiments we also observed hyperpolarization-activated currents which were inhibited by ZD7288. The amplitude of the sodium current was  $\sim 10$  times that of the other depolarizing currents and tetrodotoxin abolished action potential firing. In secretion experiments, however, nifedipine, but not tetrodotoxin,  $\omega$ -conotoxin GVIA or ZD7288, inhibited glucose-induced GLP-1 release. Consistent with this finding, the intracellular  $\text{Ca}^{2+}$  response to glucose was impaired by nifedipine but not by tetrodotoxin. Thus, in GLUTag cells, GLP-1 release is not dependent on the firing of  $\text{Na}^{+}$ -carrying action potentials but requires membrane depolarization and  $\text{Ca}^{2+}$  entry through L-type  $\text{Ca}^{2+}$  channels. Understanding the characteristics of the currents and the molecular identification of the underlying channels in GLP-1 secreting cells might facilitate the development of agents to enhance GLP-1 secretion *in vivo*.

(Received 30 September 2004; accepted after revision 15 December 2004; first published online 20 December 2004)

**Corresponding author** F. Reimann: Cambridge Institute for Medical Research, University of Cambridge, Department of Clinical Biochemistry, Wellcome Trust/MRC Building, Addenbrooke's Hospital, Hills Road, Cambridge CB2 2XY, UK.  
Email: fr222@cam.ac.uk

An early response to food ingestion is the release of hormones from enteroendocrine cells that are scattered throughout the gut epithelium. The intestinal L-cell is one such cell type secreting glucagon-like peptide-1 (GLP-1) and peptide YY (PYY) in response to dietary nutrients (Kieffer & Habener, 1999; Drucker, 2001; Stanley *et al.* 2004). As GLP-1 enhances insulin release and PYY increases satiety, agents that enhance secretion from intestinal L-cells could open novel avenues for the treatment of type 2 diabetes and obesity (Zander *et al.* 2002; Batterham *et al.* 2002). To adopt this approach it is essential that we understand the physiological events underlying L-cell function.

L-cells are distributed throughout the intestinal epithelium and are found in greatest numbers in the

more distal part of the gut, such as the ileum and colon (Eissele *et al.* 1992). In this respect they seem ill placed to directly sense nutrient delivery from the proximal gut, and it has been shown that the immediate GLP-1 response to food ingestion includes humoral and neuronal factors (Rocca & Brubaker, 1999; Anini & Brubaker, 2003). L-cells are, however, open type cells with their apical membrane being directly exposed to the luminal contents (Eissele *et al.* 1992). Pharmacological or surgical manipulations that increase the delivery of nutrients to the distal gut have been shown to increase GLP-1 and PYY secretion (Enc *et al.* 2001; Miholic *et al.* 1991), suggesting that the direct sensing of luminal nutrients might nevertheless play an important part in L-cell physiology.

The mechanisms underlying hormone release from L-cells have been studied *in vitro* using cultured fetal rat intestinal cells (Rocca & Brubaker, 1995; Brubaker *et al.* 1998), primary cultured canine intestinal cells enriched for L-cell content (Damholt *et al.* 1998), and the GLP-1 secreting cell line, GLUTag. The GLUTag cell line was derived from a colonic tumour of a transgenic mouse expressing SV40 large T antigen under the control of the proglucagon promoter (Drucker *et al.* 1994), and has been shown to secrete GLP-1 in response to a range of physiological stimuli including monosaccharides, amino acids and fatty acids (Brubaker *et al.* 1998; Reimann & Gribble, 2002; Reimann *et al.* 2004). Electrophysiological studies of L-cells have been restricted to the GLP-1 secreting cell lines because of the difficulties in distinguishing living L-cells from their neighbouring intestinal epithelial cells.

In other nutrient sensing cells, stimulus–secretion coupling usually consists of the conversion of a metabolic signal into an electrical one at the plasma membrane. This in turn triggers a rise in the cytoplasmic  $\text{Ca}^{2+}$  concentration allowing secretory vesicles to fuse with the plasma membrane (Rorsman, 1997). We have previously shown that GLUTag cells are electrically active and respond to carbohydrates and amino acids with an increase in the action potential frequency (Reimann & Gribble, 2002; Reimann *et al.* 2004). The underlying mechanism includes electrogenic sodium-coupled nutrient uptake, which directly contributes to membrane depolarization (Gribble *et al.* 2003). Metabolism of nutrients such as glucose or glutamine also results in raised cytoplasmic ATP levels, and this can depolarize the membrane due to the closure of ATP-sensitive potassium channels (Reimann & Gribble, 2002; Reimann *et al.* 2004), similar to the well established nutrient sensing mechanism in the pancreatic  $\beta$ -cell (Rorsman, 1997). Nutrient triggered GLP-1 secretion correlates with rises in the cytoplasmic  $\text{Ca}^{2+}$  concentration, supposedly due to the opening of voltage gated calcium channels. In support of this idea, it has been shown that nifedipine, a blocker of voltage gated L-type calcium channels, impairs the  $\text{Ca}^{2+}$  response of GLUTag cells on exposure to fatty acids (Sidhu *et al.* 2000). The currents underlying electrical activity in GLP-1 secreting cells have not, however, been investigated in detail. In this study we have characterized the voltage gated cation conductances that allow GLUTag cells to fire action potentials in response to nutrients.

## Methods

### Cell culture

GLUTag cells were cultured in Dulbecco's modified Eagle's medium (DMEM) containing 5.5 mM glucose (or 25 mM for cells used for microarray analysis), as previously described (Drucker *et al.* 1994; Reimann & Gribble, 2002).

### GLP-1 secretion

For secretion experiments cells were plated in Matrigel-coated 24-well culture plates, and allowed to reach 60–80% confluency. On the day of the experiment, cells were washed twice with 500  $\mu\text{l}$  nutrient-free standard bath solution supplemented with 0.1 mM DiprotinA and 0.1% (w/v) BSA. Experiments were performed by incubating the cells with test reagents in the same solution for 2 h at 37°C. The final dimethyl sulphoxide (DMSO) concentration was adjusted to 0.1% for all conditions tested, including the control. At the end of the incubation period, medium was collected and centrifuged to remove any floating cells. GLP-1 was assayed using an ELISA specific for GLP-1(7–36) amide and GLP-1(7–37) (Linco GLP-1 active ELISA-kit, Biogenesis, Poole, UK). Secretion was normalized to the baseline release in the absence of nutrients measured in parallel on the same day.

### $\text{Ca}^{2+}$ measurements

Cells were plated on Matrigel-coated coverslips 1–3 days prior to use and loaded with fura-2 by incubation in 1  $\mu\text{M}$  of the acetoxymethyl ester (Molecular Probes, Leiden, the Netherlands) for 30 min at 37°C in bath solution containing 1 mM glucose. Measurements were made after mounting the coverslip in a perfusion chamber (Warner Instruments, Harvard Apparatus) on an inverted fluorescence microscope (Olympus IX71, Southall, UK) with a 40 $\times$  oil-immersion objective. Excitation at 340 and 380 nm was achieved using a combination of a 75 W xenon arc lamp and a monochromator (Cairn Research, Faversham, UK) controlled by MetaFluor software (Universal Imaging, Cairn) and emission was recorded with a CCD camera (Orca ER, Hammamatsu, Cairn) using a dichroic mirror and a 510 nm long pass filter. Free cytoplasmic  $\text{Ca}^{2+}$  concentrations were estimated for individual cells from background-subtracted fluorescence using the equation of Grynkiewicz *et al.* (1985) assuming a  $K_D$  of 224 nM. Minimal and maximal signals were recorded in the presence of 5  $\mu\text{M}$  ionomycin in 5 mM EGTA/0 mM  $\text{Ca}^{2+}$  and 5 mM  $\text{Ca}^{2+}$ , respectively, at the end of the experiment.

### Electrophysiology

Cells were plated into 35 mm dishes 1–3 days prior to use. Experiments were performed on single cells and well-defined cells in small clusters. Microelectrodes were pulled from borosilicate glass (GC150T, Harvard Apparatus, Edenbridge, UK) and the tips coated with refined yellow beeswax. Electrodes were fire-polished using a microforge (Narishige, London) and had resistances of 2.5–3 M $\Omega$  when filled with pipette solution. Membrane potential and currents were recorded using

either an Axopatch 200B (Axon Instruments, Union City, CA, USA) linked through a Digidata 1320A interface and pCLAMP software (Axon Instruments), or using a HEKA EPC10 amplifier (Digitimer, Welwyn Garden City, UK) and Patchmaster/Pulse software (HEKA). Electrophysiological recordings were made using either the standard whole cell or perforated patch configuration of the patch clamp set-up, at 22–24°C. Standard whole-cell currents were zero and leak subtracted using HEKA pulsefit or patchmaster software and a *P/4* protocol with a holding potential of –90 mV.

### Solutions and chemicals

The standard bath solution contained (mM): 5.6 KCl, 138 NaCl, 4.2 NaHCO<sub>3</sub>, 1.2 NaH<sub>2</sub>PO<sub>4</sub>, 2.6 CaCl<sub>2</sub>, 1.2 MgCl<sub>2</sub>, 10 Hepes (pH 7.4). This was modified for the measurement of specific membrane currents, as follows. For Na<sup>+</sup> currents, K<sup>+</sup> was replaced with Cs<sup>+</sup> and Na<sup>+</sup> was partially replaced by 20 mM TEA<sup>+</sup>. The same solution was used to record Ca<sup>2+</sup> currents after the addition of 0.3 μM TTX. When Ba<sup>2+</sup> or Co<sup>2+</sup> was used, HCO<sub>3</sub><sup>-</sup> and H<sub>2</sub>PO<sub>4</sub><sup>-</sup> were additionally replaced with Cl<sup>-</sup>. To record K<sup>+</sup> currents TTX (0.3 μM) was added to the standard bath solution and Na<sup>+</sup> was partially replaced with TEA<sup>+</sup> (20 mM) as indicated. Nutrients and drugs were added to the bath solutions as indicated. Electrophysiological recordings were performed in the presence of 1 mM glucose unless otherwise indicated. The perforated patch pipette solution contained (mM): 76 K<sub>2</sub>SO<sub>4</sub>, 10 KCl, 10 NaCl, 55 sucrose, 10 Hepes, 1 MgCl<sub>2</sub> (pH 7.2); to which amphotericin B was added to a final concentration of 200 μg ml<sup>-1</sup>. The standard whole cell patch pipette solution contained (mM): 107 KCl, 1 CaCl<sub>2</sub>, 7 MgCl<sub>2</sub>, 11 EGTA, 10 Hepes, 5 K<sub>2</sub>ATP (pH 7.2 with KOH). For Na<sup>+</sup>- and Ca<sup>2+</sup>-current recordings K<sup>+</sup> was replaced by Cs<sup>+</sup> and Na<sub>2</sub>ATP was used. Drugs and chemicals were purchased from Sigma-Aldrich (Poole, UK) unless otherwise stated. ω-Conotoxin GVIA was purchased from Calbiochem (Merck Eurolab, Lutterworth, UK), ZD7288 was purchased from Tocris Cookson (Bristol, UK), CsCl and CsOH were from Alfa Aesar (Avocado Research Chemicals, Heysham, UK).

### Data analysis

Data were analysed with Origin software (OriginLab Corp. Northampton, MA, USA), using the following equations.

For voltage-dependent inactivation:

$$g/g_{\max} = (1 - A_2)/(1 + e^{(V_m - V_{0.5})/k}) + A_2 \quad (1)$$

where *g* is the conductance, *g*<sub>max</sub> is the maximum conductance, *V*<sub>m</sub> is the membrane potential, *V*<sub>0.5</sub> is the voltage at which channels are half (in-)activated, and *k* is a constant.

For voltage-dependent activation of K<sup>+</sup> channels:

$$I = \frac{g_{\max}(V_m + 80)}{1 + e^{(V_{0.5} - V_m)/k}} \quad (2)$$

For voltage-dependent activation of *I*<sub>h</sub> channels:

$$I = \frac{g_{\max(I_h)}(V_m + 40)}{1 + e^{(V_m - V_{0.5})/k}} + g_{(I, \text{background})}(V_m - V_{\text{rev}(I, \text{background})}) \quad (3)$$

in which the first term describes the *I*<sub>h</sub> current, and the second describes the background (non-*I*<sub>h</sub>) current. *g*<sub>(I, background)</sub> is the conductance of the non-*I*<sub>h</sub> current, and *V*<sub>rev(I, background)</sub> is the reversal potential of the background current. The reversal potential of *I*<sub>h</sub> was determined from the magnitude of the tail currents on stepping the potential back from –120 mV to different voltages.

### Statistical analysis

Results are presented as means ± standard error of the mean. Statistical significance was tested by Student's *t* test, using a threshold for significance of *P* < 0.05.

### Affymetrix chip microarray analyses

The GLUTag cell line was interrogated using the Affymetrix GeneChips MG\_U74Av2 (Santa Clara, CA, USA). The experiment was performed in triplicate using three independently prepared RNA samples. RNA for microarray analysis was prepared from GLUTag cells grown to 80% confluence in DMEM (high glucose) from Hyclone supplemented with 15% heat inactivated (HI) fetal calf serum (FCS; Invitrogen) and penicillin–streptomycin (Sigma). The day before RNA extraction, tissue culture medium was replaced with fresh medium. Total RNA was prepared using Trizol extraction, and RNaseasy kit (Qiagen). The chips were processed in Affymetrix Microarray Suite 5.0 (MAS5.0) using default settings (scaled to a target intensity of 150). To identify present and absent expressed genes we used signal intensity and detection *P*-value for probes corresponding to channels of interest. A putative expressed gene was designated 'absent' if the probe signal intensity was lower than 15 and if the detection *P*-value was greater than 0.3 in at least two of three replicates. Alternatively, the probe could also be designated 'absent' if signal intensity in at least two of three replicates was less than 5.

Gene expression for specific probes was designated 'present' if at least one of the following three conditions were satisfied: signal intensity greater than 10 in at least two of the three replicates and the detection *P*-value is less than 0.05 in all three replicates; signal intensity greater than 20 and detection *P*-value is less than 0.2 in at least two of three replicates; the signal intensity is greater than 45 and the detection *P*-value is less than 0.4 in at least two of three replicates.

The remaining probes (genes) that did not clearly satisfy criteria for being designated 'present' or 'absent' were called 'marginal'. The above thresholds were retrospectively derived from a previous study comparing RT-PCR analysis of GLUTag RNA with microarray data for 72 independent probes (genes). The detection thresholds were optimized to obtain the highest level of agreement between RT-PCR and microarray data with an error rate of  $\sim 10\%$  (D. Drucker, unpublished data).

### RT-PCR and Southern blot analysis

RNA was prepared from  $\alpha$ TC (a pancreatic  $\alpha$ -cell line),  $\beta$ TC (a pancreatic  $\beta$ -cell line), GluTag and STV2 (mouse embryo fibroblast, SV 40 transformed) cells using Trizol reagent (Invitrogen Canada Inc.) according to the manufacturer's instructions. First-strand cDNA synthesis was generated from total RNA using SuperScript Preamplification System (Invitrogen Canada Inc.). Target cDNAs were then amplified by PCR using specific primer pairs. The sequences for the primers and specific conditions used for RT-PCR experiments are given in the on-line Supplementary material. PCR products were loaded onto a 1% agarose gel, electrophoresed

in Tris-acetate-EDTA buffer, transferred onto nylon membranes, and hybridized using internal oligonucleotide probes labelled by T4 kinase reaction with [ $^{32}$ P]ATP (Amersham Bioscience Corp.).

### Results

As previously described, GLUTag cells were largely quiescent in the absence of nutrient, but fired action potentials when exposed to glucose or glutamine (Fig. 1). The mean resting potential in nutrient-free medium was  $-51 \pm 1$  mV ( $n = 17$ ). Action potentials were observed to overshoot to positive potentials, with a mean peak in the presence of glucose of  $+31 \pm 4$  mV ( $n = 18$ ). Lower peaks were observed when the cells fired from a more depolarized level. To measure the threshold for action potential initiation, we injected brief depolarizing currents of increasing magnitude (Fig. 1B). Action potentials were fired when the membrane potential was depolarized beyond  $-28 \pm 3$  mV ( $n = 5$ ).

### Voltage-dependent Na<sup>+</sup> channels

The overshoot of the action potential suggests the presence of large, rapidly activating, voltage-dependent inward currents. To isolate this current, we used standard whole-cell recordings with a Cs<sup>+</sup>-containing pipette solution and CsCl plus 20 mM TEA<sup>+</sup> in the bath, to block K<sup>+</sup> currents. Voltage steps (from a  $-70$  mV holding potential) triggered a rapidly inactivating inward current at potentials positive to  $-40$  mV, which was highly sensitive to tetrodotoxin (complete block at  $0.3 \mu\text{M}$  TTX), characteristic of voltage-dependent Na<sup>+</sup> currents (Fig. 2). The current-voltage ( $I$ - $V$ ) relationship showed that the Na<sup>+</sup> currents reached a peak amplitude of  $-661 \pm 113$  pA cell<sup>-1</sup> at  $+10$  mV ( $n = 13$ ). Fitting the currents with a classical Hodgkin-Huxley  $m^3h$  model revealed that both activation and inactivation were faster at more depolarized potentials. The voltage dependence of steady state inactivation was measured by holding the membrane potential at voltages between  $-120$  and  $0$  mV before stepping to a 5 ms test pulse at  $+10$  mV. The relative peak conductance of the test pulse was fitted with a Boltzmann equation (eqn (1)), giving a  $V_{0.5}$  of  $-39.7 \pm 0.7$  mV and a  $k$  of  $9.2 \pm 0.5$  mV ( $n = 12$ ).

### Voltage-dependent Ca<sup>2+</sup> currents

In the presence of TTX, a smaller voltage-dependent inward current remained (Fig. 3). This was also observed when extracellular Ca<sup>2+</sup> was replaced by Ba<sup>2+</sup>, but was totally abolished in the presence of 5 mM Co<sup>2+</sup>, characteristics typical of voltage-dependent Ca<sup>2+</sup> currents. The  $I$ - $V$  relationship, measured in 2.6 mM external Ca<sup>2+</sup>, showed that the currents were first observed

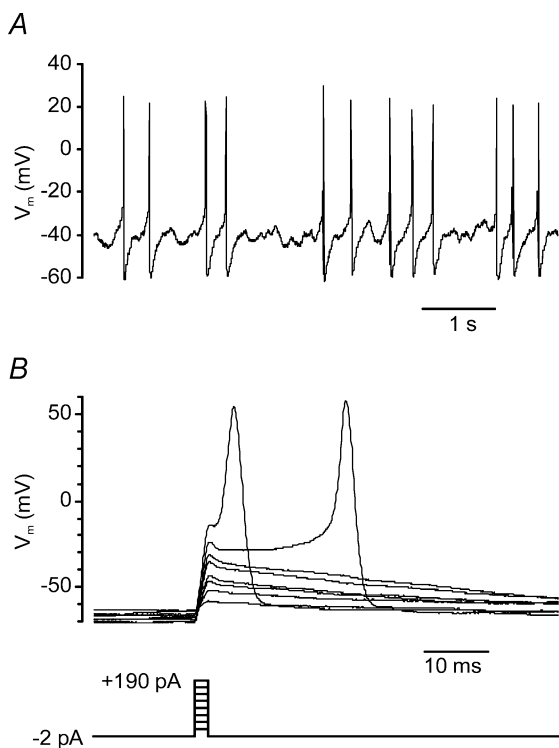


**Figure 1. Action potentials in GLUTag cells**

A, perforated patch recording of a GLUTag cell, showing action potentials in the presence of 10 mM glucose. B, measurement of the action potential threshold by injection of 2 ms depolarizing currents of increasing magnitude. The recording was made in 1 mM glucose, using the perforated patch technique. The current pulse protocol is shown at the bottom and the recorded membrane potential at the top.

at depolarizations positive to  $-50$  mV and reached a maximum amplitude of  $-72 \pm 11$  pA cell $^{-1}$  at  $0$  mV ( $n = 5$ ), measured 10–25 ms after the initiation of the voltage pulse. With  $\text{Ba}^{2+}$  as the charge carrier the  $I$ – $V$  relationship was similar but the current magnitude was slightly greater than with  $\text{Ca}^{2+}$ . Prolonged depolarization in the presence of  $\text{Ca}^{2+}$  resulted in partial inactivation of the  $\text{Ca}^{2+}$  currents which, at  $0$  mV, could be fitted with the sum of two exponentials with time constants of  $\tau_{\text{fast}} = 65 \pm 9$  ms and  $\tau_{\text{slow}} = 3 \pm 1$  s and relative amplitudes of  $A_{\text{fast}} = 38 \pm 6\%$  and  $A_{\text{slow}} = 62 \pm 6\%$ , respectively ( $n = 9$ ). The voltage dependence of steady state inactivation was determined following 5 s or 500 ms prepulses to different potentials. As both the long and

shorter prepulses had similar effects on inactivation (data not shown), the shorter protocol was used for further experiments and analysis. Inactivation appeared to be voltage dependent and could be fitted with a Boltzmann equation (eqn (1)) with a  $V_{0.5}$  of  $-25 \pm 3$  mV (Fig. 3C and D).  $\text{Ba}^{2+}$  currents were inhibited  $54 \pm 4\%$  by the L-type  $\text{Ca}^{2+}$  channel blocker, nifedipine ( $5 \mu\text{M}$ ,  $n = 11$ ), and  $31 \pm 6\%$  by the N-type  $\text{Ca}^{2+}$  channel blocker,  $\omega$ -conotoxin-GVIA ( $1 \mu\text{M}$ ,  $n = 6$ ) (Fig. 3E and F).

### K<sup>+</sup> channels

We showed previously that GLUTag cells express functional  $\text{K}_{\text{ATP}}$  channels, which play a role in glucose

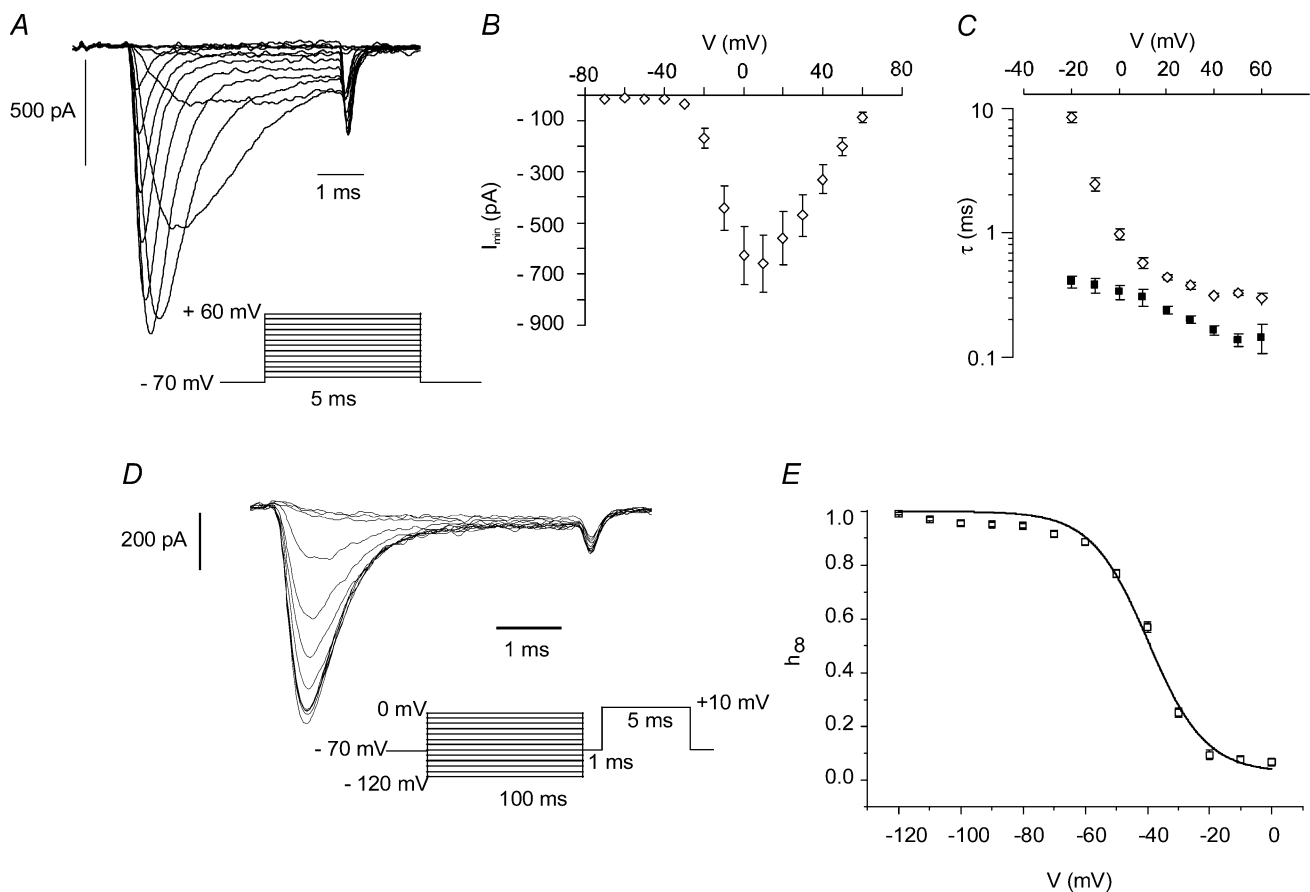
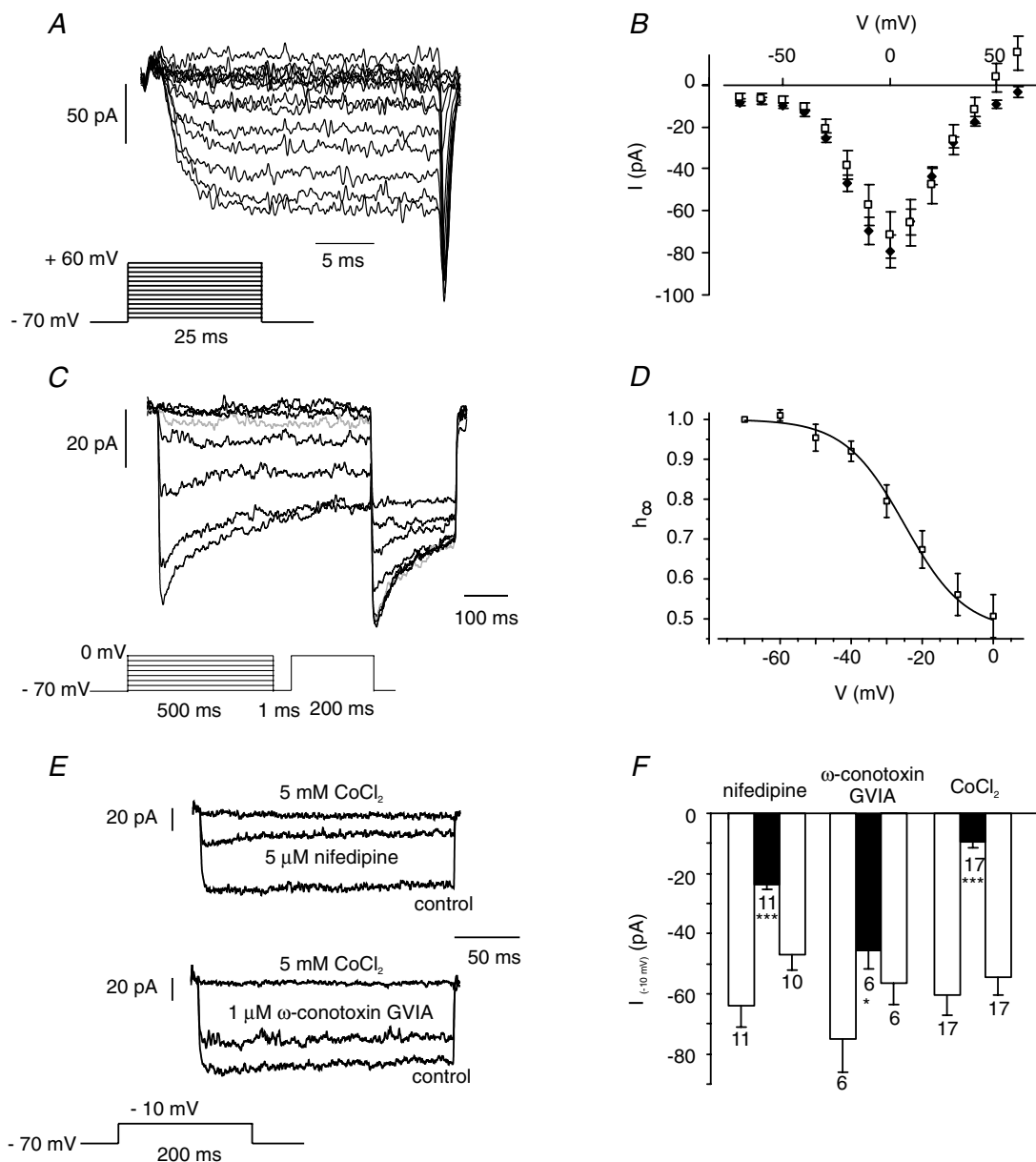


**Figure 2. Voltage gated  $\text{Na}^+$  currents**

A, current responses to 5 ms voltage steps of 10 mV increments from a holding potential of  $-70$  mV, in a whole cell voltage clamp recording applied at  $\sim 1$  Hz. The patch pipette contained  $\sim 140$  mM  $\text{Cs}^+$  and the bath contained 5.6 mM  $\text{Cs}^+$  and 20 mM  $\text{TEA}^+$  to block  $\text{K}^+$  currents. The inset shows the voltage pulse protocol. B, current–voltage relationship of the peak currents obtained using the experimental set-up shown in A ( $n = 13$ ). C, voltage dependence of the activation time constant,  $\tau_m$  ( $\diamond$ ), and inactivation time constant,  $\tau_h$  ( $\blacksquare$ ), obtained by fitting the current traces (as in A) with a Hodgkin-Huxley  $m^3 h$  model ( $n = 11$ ). D, voltage dependence of the steady state inactivation was measured by holding the membrane potential for 100 ms at conditioning voltages from  $-120$  to  $0$  mV (at 10 mV increments) before stepping to  $-70$  mV for 1 ms,  $+10$  mV for 5 ms, and then to  $-70$  mV. The inset shows the voltage pulse protocol. Only the current response to the test pulse to  $+10$  mV is shown. E, the peak currents obtained as in D ( $n = 12$ ) were normalized to the maximum peak current, and plotted against the holding potential applied during the conditioning pulse. The data were fitted with a Boltzmann equation (eqn (1):  $V_{0.5} = -39.7 \pm 0.7$  mV,  $k = 9.2 \pm 0.5$  mV,  $A_2 = 0$ ).



sensing. The presence of the Kir6.2 subunit of the  $K_{ATP}$  channel was confirmed by RT-PCR in this study. Other  $K^+$  channels in GLUTag cells were studied with 5 mM ATP in the patch pipette to block the  $K_{ATP}$  current, and with  $K^+$ -containing pipette and bath solutions. Stepping to depolarized potentials under these conditions resulted in voltage-dependent outward currents which showed partial inactivation (Fig. 4). A large proportion of this current was non-inactivating and sensitive to 20 mM TEA. This component first appeared at potentials positive to  $-30$  mV and had a  $V_h$  of  $+0.5 \pm 1.1$  mV ( $n = 13$ ). The current remaining in TEA was dominated by an inactivating component, characteristic of an A-type current, which appeared at potentials positive to  $-40$  mV (Fig. 5). It showed steady state voltage-dependent inactivation, with a  $V_{0.5}$  of  $-61 \pm 2$  mV, and a  $k$  of  $7.5 \pm 0.4$  mV, and was blocked by 4-AP (10 mM). Inactivation became progressively slower at more depolarized potentials (Fig. 5)

### Hyperpolarization activated channels

The presence of a hyperpolarization-activated current ( $I_h$ ) was suggested by the observation of a time- and voltage-dependent inward current in response to hyperpolarizing voltage steps in perforated patch recordings (Fig. 6). The magnitude of this current was markedly variable between cells. It had a reversal potential of  $-40.2 \pm 1.1$  mV ( $n = 5$ ), as determined by tail current analysis, consistent with the reported permeability ratio,  $P_{Na}/P_K$ , of 0.2, for  $I_h$  channels. Using a modified Boltzmann equation (eqn (2)) to separate the voltage-dependent and -independent components of the current, we obtained mean parameters for  $I_h$  of:  $g_{\max(I_h)} = 0.70 \pm 0.14$  nS,  $V_{0.5} = -85.7 \pm 2.3$  mV and

$k = 9.2 \pm 1.0$  mV ( $n = 5$ ).  $g_{\max(I_h)}$  was reduced by  $72 \pm 6\%$  ( $n = 4$ ) following application of the  $I_h$  inhibitor ZD7288 ( $10 \mu\text{M}$ ). The  $I$ - $V$  relationship of  $I_h$  (with the background current subtracted) is shown in Fig. 6C.

### Detection of cation channel subunits in GLUTag cells by microarray analysis

The profile of cation channel subunits expressed in GLUTag cells was examined using gene microarrays (Affymetrix), and the results are shown in Table 1. The expression of channel subunits that might correspond to the currents observed electrophysiologically were confirmed by RT-PCR (Fig. 7).

### Physiological significance

To investigate the relative functional roles of voltage gated  $Na^+$  and  $Ca^{2+}$  currents in GLUTag cells, we measured the effects of different channel inhibitors on GLP-1 release (Fig. 8). Secretion triggered by 10 mM glucose was unaffected by blocking  $Na^+$  channels with tetrodotoxin ( $0.3 \mu\text{M}$ ) or inhibiting hyperpolarization-activated channels with ZD7288 ( $10 \mu\text{M}$ ). Whereas the N-type  $Ca^{2+}$  channel blocker  $\omega$ -conotoxin GVIA ( $1 \mu\text{M}$ ) did not affect GLP-1 release, the L-type  $Ca^{2+}$  channel blocker nifedipine ( $5 \mu\text{M}$ ) largely abolished glucose-triggered secretion.

The lack of effect of TTX on GLP-1 release was surprising, and therefore investigated further. In perforated patch recordings, action potentials were fired with a frequency of  $\sim 1$  Hz (Reimann & Gribble, 2002) in the presence of glucose, and these were abolished by application of TTX (Fig. 9). When we monitored intracellular  $[Ca^{2+}]$  using fura-2 fluorescence, however, we

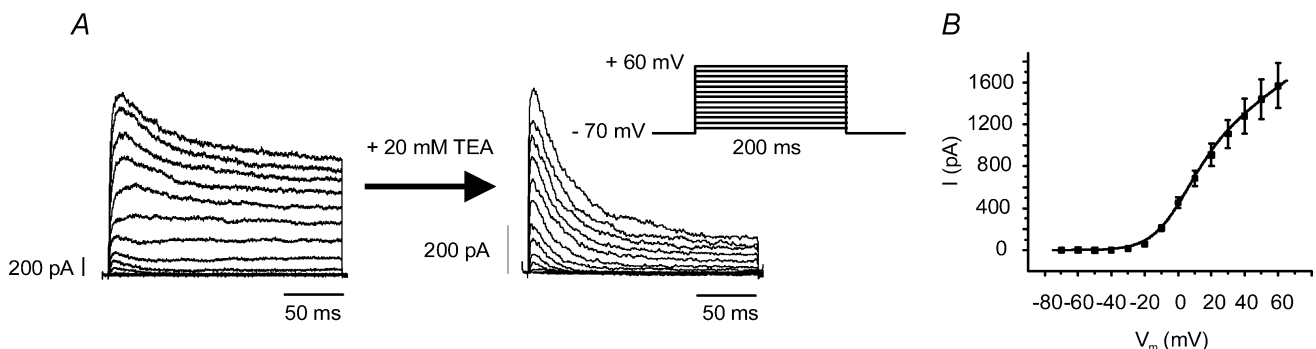


**Figure 4. Delayed outwardly rectifying  $K^+$  currents**

A, current responses to 200 ms voltage steps of 10 mV increments from a holding potential of  $-70$  mV, in a whole-cell voltage-clamp recording applied at  $\sim 1$  Hz in the presence of  $0.3 \mu\text{M}$  TTX before (left) and after (right) addition of 20 mM  $\text{TEA}^+$  to the bath. The inset shows the voltage pulse protocol. B, current-voltage relationship of the sustained  $\text{TEA}^+$ -sensitive current calculated by subtracting the mean steady state current in  $\text{TEA}^+$  from the mean steady state current before the addition of  $\text{TEA}^+$ . The data were fitted with a Boltzmann equation (eqn (2)):  $V_{0.5} = 0.5 \pm 1.1$  mV,  $k = 11.2 \pm 0.5$  mV,  $n = 13$ .

found that TTX did not prevent the rise in  $[Ca^{2+}]$  triggered by 10 mM glucose (Fig. 10). Consistent with this finding, the time-averaged mean membrane potential in the presence of glucose was not significantly affected by TTX despite the loss of action potential firing ( $-39 \pm 2$  mV in glucose plus TTX *versus*  $-38 \pm 2$  mV in glucose alone;  $n = 6$ , each). It therefore appears that the mean membrane potential is of greater importance than the presence of action potentials for glucose-triggered GLP-1 release in GLUTag cells. Nifedipine ( $10 \mu\text{M}$ ), by contrast, reduced the firing frequency but did not completely abolish the action potentials (Fig. 9), and had no effect on the mean membrane potential ( $-37 \pm 1$  mV in nifedipine/glucose *versus*  $-38 \pm 1$  mV in glucose,  $n = 5$ ). Nifedipine or a combination of nifedipine and  $\omega$ -conotoxin GVIA, strongly impaired the  $Ca^{2+}$  response to 10 mM glucose as measured with fura-2 (Fig. 10).

## Discussion

In this paper we show that GLUTag cells express a range of voltage-gated cation channels, consistent with our previous reports that these cells are electrically excitable.

### Correlation between electrophysiology and expression profiling

Expression profiling using Affimetrix gene microarrays revealed that GLUTag cells express a number of channels that would correlate with the observed electrophysiological properties. The properties of the voltage-dependent  $Na^+$  current could correspond to  $Na_v1.1$  or  $Na_v1.6$  channels encoded by *scn1a* or *scn8a* together with the  $\beta$ -subunit encoded by *scn1b* (Goldin, 2001), which were all detected on the chip. Expression of *scn8a* and *scn1b* was confirmed

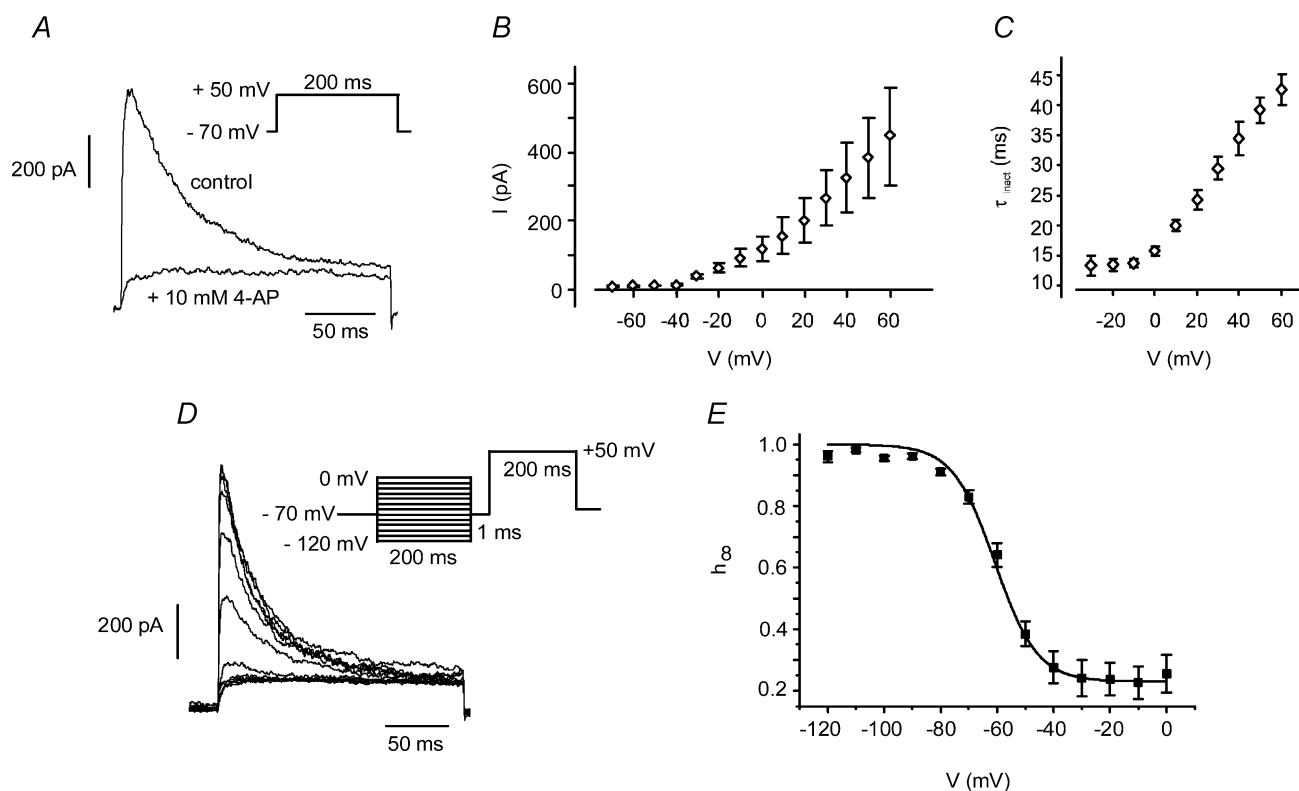


**Figure 5. A-type  $K^+$  currents**

*A*, current responses to 200 ms voltage steps to +50 mV from a holding potential of  $-70$  mV (voltage pulse protocol shown in the inset) in the presence of  $0.3 \mu\text{M}$  TTX and  $20 \text{ mM}$   $TEA^+$  before and after the addition of  $10 \text{ mM}$  4-aminopyridine. Similar results were seen in 7 cells. *B*, peak current–voltage relationship of currents after the subtraction of the mean sustained current obtained using the experimental set-up shown in Fig. 4A in the presence of  $TEA^+$  ( $n = 11$ ). *C*, voltage dependence of the inactivation time constant,  $\tau_{\text{inact}}$ , obtained by fitting the declining phase of the current traces (as in Fig. 4A) with a single exponential ( $n = 5$  to 12). *D*, voltage-dependent inactivation was measured by holding the membrane potential for 200 ms at conditioning voltages from  $-120$  to  $0$  mV (at  $10$  mV increments) before stepping to  $-70$  mV for 1 ms,  $+50$  mV for 200 ms, and then to  $-70$  mV. The voltage pulse protocol is shown in the inset. Only the current response to the test pulse to  $+50$  mV is shown. *E*, the peak currents obtained as in *D* ( $n = 9$ ) were normalized to the maximum peak current, and plotted against the holding potential applied during the conditioning pulse. The data were fitted with a Boltzmann equation (eqn (1),  $V_{0.5} = -61 \pm 2$  mV,  $k = 7.5 \pm 0.4$  mV,  $A_2 = 0$ ).

by RT-PCR. However, not all known genes encoding voltage gated sodium channel  $\alpha$ -subunits were on the Affimetrix chip (see Table 1). Of these, *scn5a* and *scn11a* are unlikely candidates for the  $\text{Na}^+$  current in GLUTag cells as they show only weak sensitivity to TTX, and *scn4a* is thought to be expressed specifically in muscle, leaving only *scn2a* as an alternative candidate. However, whilst the observed currents are most likely to reflect the expression of detected subunits, we also cannot exclude contributions from non-detected genes, as channel subunits that are expressed in GLUTag cells might escape detection with the microarray technique due to a low steady state mRNA level. This is exemplified by the 'marginal' call for the potassium channel gene *kcnj11* encoding the Kir6.2 subunit of the  $\text{K}_{\text{ATP}}$  channel, which was nevertheless detected by RT-PCR and has been shown previously to play a role in glucose sensing by GLUTag cells (Reimann & Gribble, 2002).

Genes corresponding to both L-type and N-type  $\text{Ca}^{2+}$  channels were also detected on the chip and confirmed by RT-PCR. *cacna1C* and *cacna1B* encode the  $\alpha_1$  subunits of  $\text{Ca}_v1.2$  and  $\text{Ca}_v2.2$ , respectively (Catterall, 2000). The  $\text{Ca}_v1$  channel family forms the classical L-type  $\text{Ca}^{2+}$  channels,

and the expression of  $\text{Ca}_v1.2$  could explain the L-type  $\text{Ca}^{2+}$  current in the GLUTag cells, although the alternative L-type  $\text{Ca}^{2+}$  channel subunit,  $\text{Ca}_v1.3$ , was not represented on the chip.  $\text{Ca}_v2.2$  channels make N-type  $\text{Ca}^{2+}$  currents, consistent with the finding that a proportion of the  $\text{Ca}^{2+}$  current was sensitive to  $\omega$ -conotoxin GVIA.

A range of genes encoding voltage gated potassium channels (Gutman *et al.* 2003) were found to be expressed by the GLUTag cell line (Table 1). Many of these are thought to conduct delayed activated outwardly rectifying potassium currents and are highly sensitive to  $\text{TEA}^+$ . Both  $\alpha$ -dendrotoxin (200 nM) and iberiotoxin (100 nM) only marginally blocked the whole cell voltage-dependent delayed potassium current (data not shown), excluding  $\text{K}_v1.2$ ,  $\text{K}_v1.6$  and  $\text{Kcnma1}$  (BK) as the main contributors to the TEA-sensitive current in GLUTag cells. The properties of the TEA-insensitive A-type current suggest that it might be attributable to  $\text{K}_v4.2$ , which was detected on the gene microarray and by RT-PCR, although this is not the only possible candidate, as  $\text{K}_v4.1$  was also marginally detected, and inactivation of  $\text{K}_v$  channels is strongly influenced by the expression of ancillary subunits, not

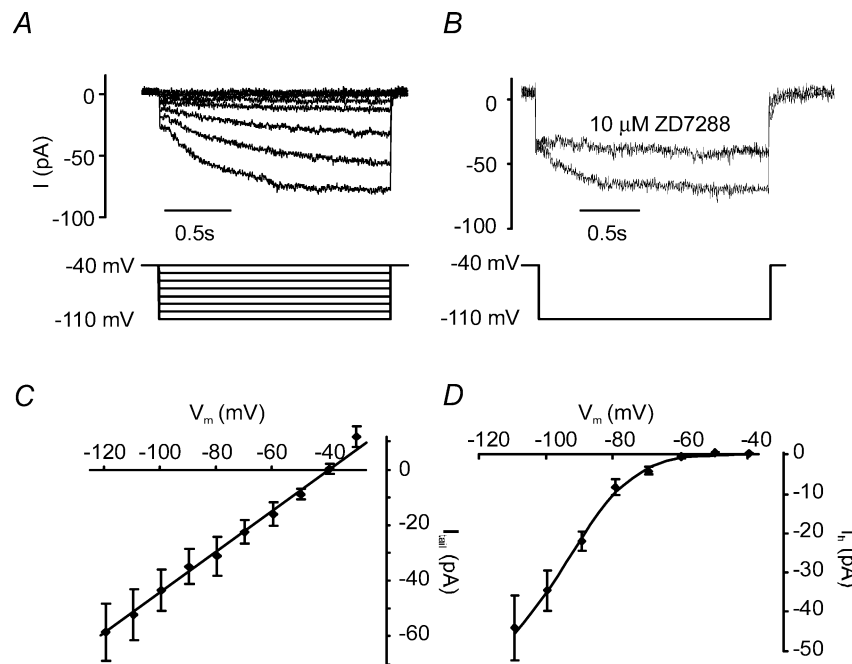


**Figure 6. Hyperpolarization activated currents ( $I_h$ )**

A, current responses to 2000 ms voltage steps of  $-10$  mV increments from a holding potential of  $-40$  mV, in a perforated patch voltage clamp recording applied at  $\sim 0.25$  Hz. The voltage pulse protocol is shown at the bottom. B, current responses to 2000 ms voltage steps to  $-110$  mV from a holding potential of  $-40$  mV before and during the addition of  $10 \mu\text{M}$  ZD7288 to the bath solution. The voltage pulse protocol is shown at the bottom. C, current-voltage relationship of tail currents obtained during a 100 ms pulse to voltages between  $-120$  and  $-30$  mV after a 2 s conditioning pulse to  $-120$  mV from a holding potential of  $-40$  mV. Data represent the average of 5 cells and were fitted with a straight line. D,  $I$ - $V$  relationship for the voltage-activated component of the currents measured in A. Data represent the average of 5 cells. The mean current at the end of the voltage step was fitted with the modified Boltzmann equation (eqn (3),  $V_{0.5} = -85.7 \pm 2.3$  mV,  $k = 9.2 \pm 1.0$  mV,  $g_{\text{max}} = 0.70 \pm 0.14$  nS), and the voltage-independent component was subtracted from the total current to display the  $I_h$  component alone.

**Table 1. Detection of genes encoding cation channels by Affymetrix chip**

	Gene name	Channel name	Detection
<b>Sodium channels</b>			
$\alpha$ -Subunits	<i>scn1a</i>	Na <sub>v</sub> 1.1	present low
	<i>scn3a</i>	Na <sub>v</sub> 1.3	absent
	<i>scn7a</i>	Na <sub>v</sub> 2.3	absent
	<i>scn8a</i>	Na <sub>v</sub> 1.6	marginal/absent
	<i>scn9a</i>	Na <sub>v</sub> 1.7	absent
	<i>scn10a</i>	Na <sub>v</sub> 1.8	absent
Ancillary subunits	<i>scn1b</i>		present/marginal
<b>Calcium channels</b>			
$\alpha$ -Subunits	<i>cacna1s</i>	Ca <sub>v</sub> 1.1, L-type	absent
	<i>cacna1c</i>	Ca <sub>v</sub> 1.2, L-type	present
	<i>cacna1a</i>	Ca <sub>v</sub> 2.1, P/Q-type	absent
	<i>cacna1b</i>	Ca <sub>v</sub> 2.2, N-type	present
	<i>cacna1e</i>	Ca <sub>v</sub> 2.3, R-type	absent
	<i>cacna1g</i>	Ca <sub>v</sub> 3.1, T-type	absent
	<i>cacna1h</i>	Ca <sub>v</sub> 3.2, T-type	absent
Ancillary subunits	<i>cacna2d1</i>	$\alpha$ 2 $\delta$ 1	present
	<i>cacna2d3</i>	$\alpha$ 2 $\delta$ 3	present
	<i>cacnb2</i>	$\beta$ 2	present
	<i>cacnb3</i>	$\beta$ 3	present
	<i>cacng1</i>	$\gamma$ 1	marginal
	<i>cacng2</i>	$\gamma$ 2	absent
	<i>Pr1</i>	$\gamma$ -like protein	absent
<b>Potassium channels</b>			
Shaker-like	<i>kcna1</i>	K <sub>v</sub> 1.1	absent
	<i>kcna2</i>	K <sub>v</sub> 1.2	marginal
	<i>kcna3</i>	K <sub>v</sub> 1.3	present/marginal
	<i>kcna4</i>	K <sub>v</sub> 1.4	absent
	<i>kcna5</i>	K <sub>v</sub> 1.5	absent
	<i>kcna6</i>	K <sub>v</sub> 1.6	marginal
	<i>kcna7</i>	K <sub>v</sub> 1.7	absent
Shab-like	<i>kcnb1</i>	K <sub>v</sub> 2.1	present
	<i>kcns1</i>	K <sub>v</sub> 9.1	marginal
	<i>kcns2</i>	K <sub>v</sub> 9.2	present
Shaw-like	<i>kcnc1</i>	K <sub>v</sub> 3.1	marginal
	<i>kcnc3</i>	K <sub>v</sub> 3.3	marginal
Shal-like	<i>kcnd1</i>	K <sub>v</sub> 4.1	marginal
	<i>kcnd2</i>	K <sub>v</sub> 4.2	present
	<i>kcnd3</i>	K <sub>v</sub> 4.3	absent
Eag-family	<i>kcnh1</i>	K <sub>v</sub> 10.1, eag1	absent
	<i>kcnh2</i>	K <sub>v</sub> 11.1, erg1	present
KCNQ-family	<i>kcng1</i>	K <sub>v</sub> 7.1, KvLQT1	present/absent
	<i>kcng2</i>	K <sub>v</sub> 7.2, M-current	present
Calcium-activated	<i>kcnn1</i>	K <sub>Ca</sub> 2.1, S <sub>KCa</sub> 1	marginal
	<i>kcnn4</i>	K <sub>Ca</sub> 3.1, I <sub>KCa</sub> 1	marginal
	<i>kcma1</i>	K <sub>Ca</sub> 1.1, BK, slo	present
	<i>kcma3</i>	slo3	absent
(ancillary subunits)	<i>kcnab1</i>	$\beta$ -Subunit	absent
	<i>kcnab2</i>	$\beta$ -Subunit	present
	<i>kcnab3</i>	$\beta$ -Subunit	present
	<i>kcne1</i>	MinK, Isk	absent
	<i>kcne1-l</i>	MiRP4	absent
	<i>kcnmb1</i>	$\beta$ -subunit	absent

*(continued)*

Table 1. continued

	Gene name	Channel name	Detection
Inward rectifiers	<i>kcnj1</i>	K <sub>ir</sub> 1.1	absent
	<i>kcnj2</i>	K <sub>ir</sub> 2.1	absent
	<i>kcnj12</i>	K <sub>ir</sub> 2.2	marginal
	<i>kcnj4</i>	K <sub>ir</sub> 2.3	present
	<i>kcnj3</i>	K <sub>ir</sub> 3.1	absent
	<i>kcnj6</i>	K <sub>ir</sub> 3.2	absent/marginal
	<i>kcnj9</i>	K <sub>ir</sub> 3.3	present
	<i>kcnj5</i>	K <sub>ir</sub> 3.4	absent
	<i>kcnj15</i>	K <sub>ir</sub> 4.2	absent
	<i>kcnj8</i>	K <sub>ir</sub> 6.1	absent
	<i>kcnj11</i>	K <sub>ir</sub> 6.2	marginal
2-pore K-channels	<i>kcnk1</i>	K <sub>2p</sub> 1.1, TWIK-1	present
	<i>kcnk2</i>	K <sub>2p</sub> 2.1, TREK-1	present
	<i>kcnk3</i>	K <sub>2p</sub> 3.1, TASK-1	absent
	<i>kcnk4.1</i>	K <sub>2p</sub> 4.1, TRAAK	marginal
	<i>kcnk7</i>	K <sub>2p</sub> 7.1	present
Non-selective cation channels			
Hyperpolarization-activated	<i>hcn1</i>	HCN1	present
	<i>hcn2</i>	HCN2	present
	<i>hcn3</i>	HCN3	present
Cyclic-nucleotide-gated	<i>cnga1</i>		absent
	<i>cnga2</i>		absent
	<i>cnga3</i>		absent
Trp channels	<i>trpv2</i>		present
	<i>trpc1</i>		present/absent
	<i>trpc4</i>		present
	<i>trpc4ap</i>		present
	<i>trpc5</i>		absent
	<i>trpc6</i>		absent
	<i>trpm1</i>		present
	<i>trpm7</i>		marginal
	<i>nscn1</i>		marginal
	<i>pkd1</i>		present
	<i>pkd2</i>		present

all of which were represented on the chip. Three genes encoding hyperpolarization-activated channels (HCN1, HCN2 and HCN3) were detected on the chip and by RT-PCR. Expression of one or more of these genes could account for the  $I_h$  current detected electrophysiologically (Robinson & Siegelbaum, 2003).

#### How might the different channels contribute to action potential firing?

GLUtag cells were found to express a large functional voltage-dependent  $\text{Na}^+$  current, which activated at membrane potentials close to the action potential threshold, and which showed strong voltage-dependent inactivation at membrane potentials between  $-50$  and  $-20$  mV. Consistent with the voltage dependency of  $\text{Na}^+$  channel inactivation, the action potential peak was also observed to diminish when the membrane potential

during the interspike interval was more depolarized. Blocking the  $\text{Na}^+$  channels with TTX abolished action potential firing, indicating that they play a prominent role in forming the upstroke of the action potentials. The voltage gated  $\text{Ca}^{2+}$  current, by contrast, was approximately 10 times smaller than the  $\text{Na}^+$  current, but activated at slightly more negative potentials. Blocking the L-type  $\text{Ca}^{2+}$  current with nifedipine reduced the action potential frequency, but did not abolish firing completely. This might be explained if the opening of  $\text{Ca}^{2+}$  channels contributes to an initial depolarization, bringing the membrane potential towards the threshold for  $\text{Na}^+$  channel activation, and thereby enhancing the probability of firing an action potential.

The voltage-gated  $\text{K}^+$  current consisted of a mixture of currents, as has been reported for other excitable tissues (Hille, 2001). Delayed rectifier channels were only observed at voltages positive to  $\sim -20$  mV, but would be

strongly activated during an action potential. This might account for the after-hyperpolarization observed when the action potentials overshoot strongly. A-type currents, by contrast, activated at membrane potentials positive to  $-40$  mV, but were largely inactivated by  $-30$  mV. In other pacemaker tissues, A-type currents are believed to allow modulation of the action potential frequency, as they act as a brake on the rate of depolarization during the interspike interval. This might therefore allow GLUTag cells to control their firing frequency. The latter could also be modulated by the observed  $I_h$  current, which would only be activated during the after-hyperpolarization of action potentials (Robinson & Siegelbaum, 2003).

### Effect of $\text{Na}^+$ and $\text{Ca}^{2+}$ channel blockade on GLP-1 release

Despite the necessity of voltage-gated  $\text{Na}^+$  channels for the firing of the characteristic overshooting action potentials, TTX did not prevent the glucose-triggered rise in intracellular  $[\text{Ca}^{2+}]$  or GLP-1 release. The most likely explanation for this finding is that the action potentials are very brief relative to the interspike interval because of the low firing frequency ( $\sim 1$  Hz), and are followed by a 5–10 times longer after-hyperpolarization. As a result, the mean membrane potential in the presence of glucose was largely unaffected by the firing of action potentials and although additional  $\text{Ca}^{2+}$  channels would be recruited during an action potential, this would be followed by a longer period during which they would be deactivated, and  $\text{Ca}^{2+}$  entry correspondingly reduced. As

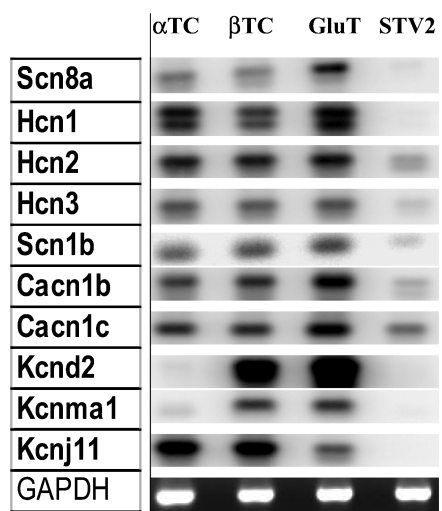


**Figure 7. RT-PCR detection of channel subunit expression**  
 $\alpha$ TC-1,  $\beta$ TC-6, STV2 and GLUTag cells were grown to 80% confluence and RNA was extracted for RT-PCR analysis as described in Methods. Following RT-PCR, Southern blots were hybridized with internal oligonucleotide probes specific for each ion channel mRNA transcript. The gene nomenclature corresponds to that given in Table 1.

glucose depolarized the cells from  $\sim -50$  to  $\sim -40$  mV in both the presence and absence of TTX, the sustained  $\text{Ca}^{2+}$  current detected during prolonged depolarizations to  $-40$  mV could account for the glucose-triggered rise in intracellular  $[\text{Ca}^{2+}]$  and GLP-1 release that was observed even in the presence of TTX.

The electrophysiological and molecular biological identification of L-type  $\text{Ca}^{2+}$  channels and their functional importance in GLP-1 release from GLUTag cells is not surprising. These types of channel have been implicated in  $\text{Ca}^{2+}$  entry and hormone/neurotransmitter release in a variety of cell types, including pancreatic  $\alpha$ - and  $\beta$ -cells (Rorsman & Trube, 1986; Bokvist *et al.* 1995; Gromada *et al.* 1997; Gopel *et al.* 2004). It has also been shown previously that the  $\text{Ca}^{2+}$  transients triggered by fatty acids in GLUTag cells are sensitive to inhibition by L-type  $\text{Ca}^{2+}$  channel blockers (Sidhu *et al.* 2000). We also identified a second component of the  $\text{Ca}^{2+}$  current in GLUTag cells that was sensitive to  $\omega$ -conotoxin GVIA, identifying it as an N-type  $\text{Ca}^{2+}$  current. Consistent with these findings, although nifedipine largely impaired the cytoplasmic  $[\text{Ca}^{2+}]$  response to glucose, a combination of nifedipine and  $\omega$ -conotoxin GVIA reduced the response even further. The data support the idea that  $\text{Ca}^{2+}$  entry through both voltage gated L- and N-type  $\text{Ca}^{2+}$  channels underlies the cytoplasmic  $\text{Ca}^{2+}$  response to glucose. However, whereas blocking L-type  $\text{Ca}^{2+}$  channels

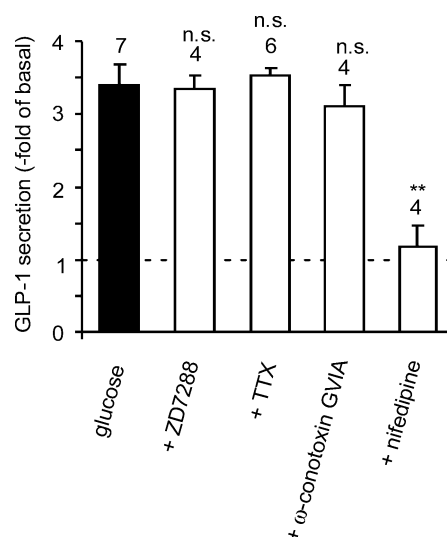


**Figure 8. Pharmacological modulation of glucose triggered GLP-1 secretion**

GLP-1 secretion from GLUTag cells incubated for 2 h with 10 mM glucose or 10 mM glucose plus ZD7288 ( $10 \mu\text{M}$ ), TTX ( $0.3 \mu\text{M}$ ),  $\omega$ -conotoxin GVIA ( $1 \mu\text{M}$ ) or nifedipine ( $5 \mu\text{M}$ ) as indicated. Secretion was normalized to baseline secretion in the absence of nutrients, measured in parallel on the same day. The number of wells is indicated above each bar. Statistical significance comparing secretion in 10 mM glucose with and without inhibitor was tested using Student's *t* test,  $**P < 0.01$ , n.s. = non significant.

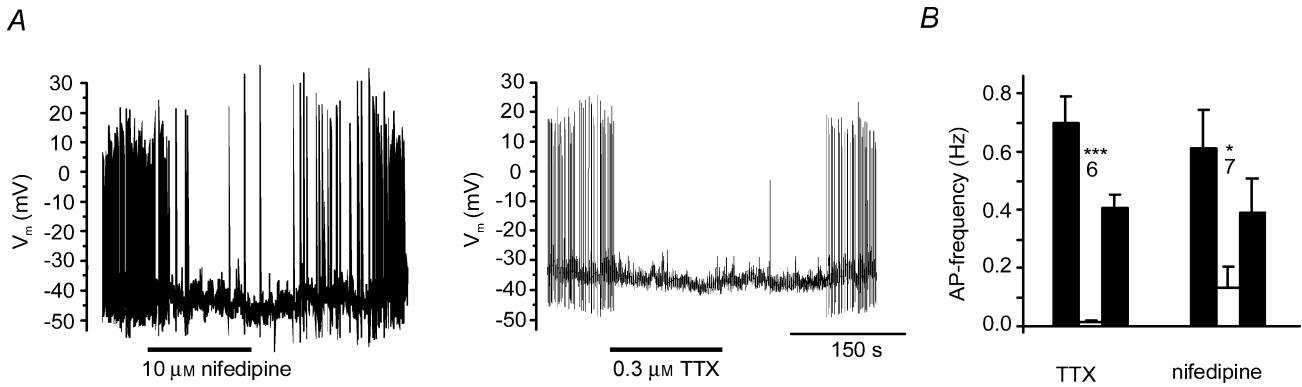


**Figure 9. Pharmacological modulation of glucose triggered action potentials**

A, perforated patch recording of a GLUTag cell, showing action potentials in the presence of 10 mM glucose are partially or completely abolished by the addition of 10  $\mu$ M nifedipine (left) or 0.3  $\mu$ M TTX (right). B, action potential frequency recorded as in A in the presence of 10 mM glucose before (filled bars), during (unfilled bars) and after (filled bars) addition of 0.3  $\mu$ M TTX or 10  $\mu$ M nifedipine. The number of cells is indicated above the bars. Error bars represent 1 s.e.m. and significance was tested using Student's *t* test: \*\*\**P* < 0.001, \**P* < 0.05.

with nifedipine abolished glucose-triggered GLP-1 release, blocking N-type  $Ca^{2+}$  channels did not impair secretion, emphasizing a predominant role of L-type  $Ca^{2+}$  channels in the pathways controlling glucose-stimulated hormone secretion from GLUTag cells. In pancreatic  $\beta$ -cells, a similar strong dependence of exocytosis on  $Ca^{2+}$  entry through L-type  $Ca^{2+}$  channels has been attributed to a physical interaction between the tail of the L-type  $Ca^{2+}$  channel and the exocytotic vesicles (Barg *et al.* 2002). As N-type  $Ca^{2+}$  channels are known to undergo voltage-dependent inactivation (Hille, 2001), a simple explanation for these results could have been that the N-type current is completely inactivated when the membrane experiences a prolonged depolarization in the presence of glucose (typically to  $\sim -40$  mV). This

idea was not, however, supported by measurements of the voltage dependence of  $Ca^{2+}$  channel inactivation, which revealed that inactivation only became significant following prolonged depolarizations beyond  $-30$  mV. It is possible that N-type  $Ca^{2+}$  channels, although not apparently contributing to glucose-triggered GLP-1 release, might play more important roles under other conditions. In this respect it is interesting that the relative roles of L-type and N-type  $Ca^{2+}$  channels in triggering glucagon release from pancreatic  $\alpha$ -cells appear to depend on the specific stimuli and experimental conditions (Gromada *et al.* 1997).

In summary, we have shown that GLUTag cells express a range of voltage-dependent cation channels which play a role in the firing of action potentials. The

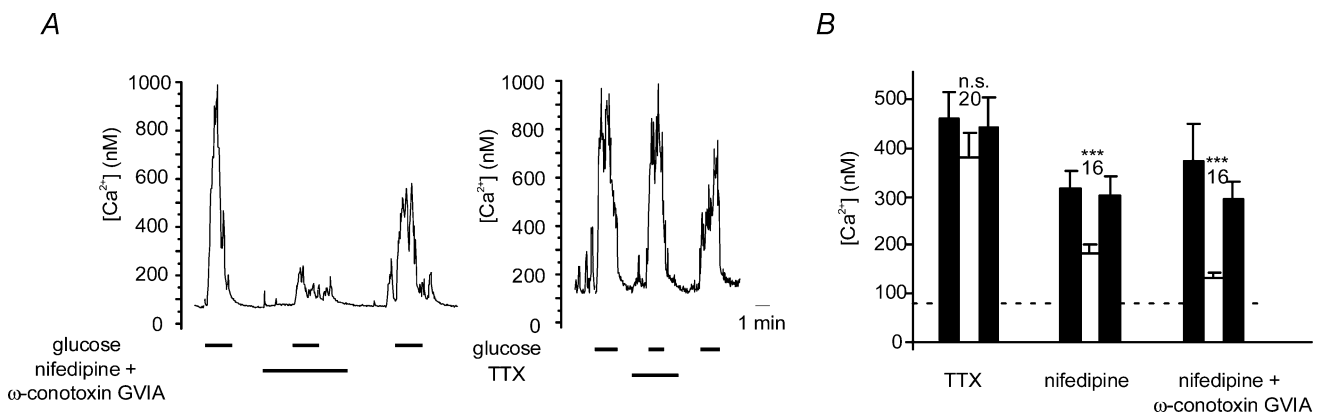


**Figure 10. Pharmacological modulation of glucose triggered  $[Ca^{2+}]_i$  responses**

A, cytoplasmic  $Ca^{2+}$  concentration ( $[Ca^{2+}]_i$ ) in a single cell in response to 10 mM glucose in the absence or presence of 5  $\mu$ M nifedipine + 1  $\mu$ M  $\omega$ -conotoxin GVIA or 0.3  $\mu$ M TTX as indicated. B, mean  $[Ca^{2+}]_i$  measured during a 30-s period during the application of 10 mM glucose before (filled bars), during (unfilled bars) and after (filled bars) addition of 0.3  $\mu$ M TTX, 5  $\mu$ M nifedipine or 5  $\mu$ M nifedipine + 1  $\mu$ M  $\omega$ -conotoxin GVIA. The number of cells is indicated above the bars. Error bars represent 1 s.e.m. and significance was tested using Student's *t* test comparing the response to 10 mM glucose in the presence of drugs to the mean response before and after drug application: n.s. = non significant, \*\*\**P* < 0.001.

most critical factor in determining GLP-1 secretion, however, appears to be membrane depolarization and the opening of L-type  $\text{Ca}^{2+}$  channels, rather than the action potential firing itself. Understanding the currents underlying hormone secretion from enteroendocrine cells may contribute to the targeted development of drugs to enhance secretion *in vivo*, and that might therefore be used in the treatment of diabetes and obesity.

## References

- Anini Y & Brubaker PL (2003). Muscarinic receptors control glucagon-like peptide 1 secretion by human endocrine L cells. *Endocrinology* **144**, 3244–3250.
- Barg S, Eliasson L, Renstrom E & Rorsman P (2002). A subset of 50 secretory granules in close contact with L-type  $\text{Ca}^{2+}$  channels accounts for first-phase insulin secretion in mouse  $\beta$ -cells. *Diabetes* **51**, S74–S82.
- Batterham RL, Cowley MA, Small CJ, Herzog H, Cohen MA, Dakin CL *et al.* (2002). Gut hormone PYY (3–36) physiologically inhibits food intake. *Nature* **418**, 650–654.
- Bokvist K, Eliasson L, Ammala C, Renstrom E & Rorsman P (1995). Co-localization of L-type  $\text{Ca}^{2+}$  channels and insulin-containing secretory granules and its significance for the initiation of exocytosis in mouse pancreatic B-cells. *EMBO J* **14**, 50–57.
- Brubaker PL, Schloos J & Drucker DJ (1998). Regulation of glucagon-like peptide-1 synthesis and secretion in the GLUTag enteroendocrine cell line. *Endocrinology* **139**, 4108–4114.
- Catterall WA (2000). Structure and regulation of voltage-gated  $\text{Ca}^{2+}$  channels. *Annu Rev Cell Dev Biol* **16**, 521–555.
- Damholt AB, Buchan AM & Kofod H (1998). Glucagon-like-peptide-1 secretion from canine I-cells is increased by glucose-dependent-insulinotropic peptide but unaffected by glucose. *Endocrinology* **139**, 2085–2091.
- Drucker DJ (2001). Minireview: the glucagon-like peptides. *Endocrinology* **142**, 521–527.
- Drucker DJ, Jin T, Asa SL, Young TA & Brubaker PL (1994). Activation of proglucagon gene transcription by protein kinase A in a novel mouse enteroendocrine cell line. *Mol Endocrinol* **8**, 1646–1655.
- Eissele R, Goke R, Willemer S, Harthus HP, Vermeer H, Arnold R *et al.* (1992). Glucagon-like peptide-1 cells in the gastrointestinal tract and pancreas of rat, pig and man. *Eur J Clin Invest* **22**, 283–291.
- Enc FY, Imeryuz N, Akin L, Turoglu T, Dede F, Haklar G *et al.* (2001). Inhibition of gastric emptying by acarbose is correlated with GLP-1 response and accompanied by CCK release. *Am J Physiol* **281**, G752–G763.
- Goldin AL (2001). Resurgence of sodium channel research. *Annu Rev Physiol* **63**, 871–894.
- Gopel S, Zhang Q, Eliasson L, Ma XS, Galvanovskis J, Kanno T *et al.* (2004). Capacitance measurements of exocytosis in mouse pancreatic alpha-, beta- and delta-cells within intact islets of Langerhans. *J Physiol* **556**, 711–726.
- Gribble FM, Williams L, Simpson AK & Reimann F (2003). A novel glucose-sensing mechanism contributing to Glucagon-Like Peptide-1 secretion from the GLUTag cell line. *Diabetes* **52**, 1147–1154.
- Gromada J, Bokvist K, Ding WG, Barg S, Buschard K, Renstrom E *et al.* (1997). Adrenaline stimulates glucagon secretion in pancreatic A-cells by increasing the  $\text{Ca}^{2+}$  current and the number of granules close to the L-type  $\text{Ca}^{2+}$  channels. *J General Physiol* **110**, 217–228.
- Gryniewicz G, Poenie M & Tsien RY (1985). A new generation of  $\text{Ca}^{2+}$  indicators with greatly improved fluorescence properties. *J Biol Chem* **260**, 3440–3450.
- Gutman GA, Chandy KG, Adelman JP, Aiyar J, Bayliss DA, Clapham DE *et al.* (2003). International Union of Pharmacology. XLI. Compendium of voltage-gated ion channels: potassium channels. *Pharmacol Rev* **55**, 583–586.
- Hille B (2001). *Ion Channels of Excitable Membranes*. Sinauer Associates, Inc, Sunderland, MA.
- Kieffer TJ & Habener JF (1999). The glucagon-like peptides. *Endocr Rev* **20**, 876–913.
- Miholic J, Orskov C, Holst JJ, Kotzerke J & Meyer HJ (1991). Emptying of the gastric substitute, glucagon-like peptide-1 (GLP-1), and reactive hypoglycemia after total gastrectomy. *Dig Dis Sci* **36**, 1361–1370.
- Reimann F & Gribble FM (2002). Glucose sensing in GLP-1 secreting cells. *Diabetes* **51**, 2757–2763.
- Reimann F, Williams L, Silva Xavier G, Rutter GA & Gribble FM (2004). Glutamine potently stimulates glucagons-like peptide-1 secretion from GLUTag cells. *Diabetologia* **47**, 1592–601.
- Robinson RB & Siegelbaum SA (2003). Hyperpolarization-activated cation currents: from molecules to physiological function. *Annu Rev Physiol* **65**, 453–480.
- Rocca AS & Brubaker PL (1995). Stereospecific effects of fatty acids on proglucagon-derived peptide secretion in fetal rat intestinal cultures. *Endocrinology* **136**, 5593–5599.
- Rocca AS & Brubaker PL (1999). Role of the vagus nerve in mediating proximal nutrient-induced glucagon-like peptide-1 secretion. *Endocrinology* **140**, 1687–1694.
- Rorsman P (1997). The pancreatic beta-cell as a fuel sensor: an electrophysiologist's viewpoint. *Diabetologia* **40**, 487–495.
- Rorsman P & Trube G (1986). Calcium and delayed potassium currents in mouse pancreatic beta-cells under voltage-clamp conditions. *J Physiol* **374**, 531–550.
- Sidhu SS, Thompson DG, Warhurst G, Case RM & Benson RS (2000). Fatty acid-induced cholecystokinin secretion and changes in intracellular  $\text{Ca}^{2+}$  in two enteroendocrine cell lines, STC-1 and GLUTag. *J Physiol* **528**, 165–176.
- Stanley S, Wynne K & Bloom S (2004). Gastrointestinal satiety signals III. Glucagon-like peptide 1, oxyntomodulin, peptide YY, and pancreatic polypeptide. *Am J Physiol* **286**, G693–G697.
- Zander M, Madsbad S, Madsen JL & Holst JJ (2002). Effect of 6-week course of glucagon-like peptide 1 on glycaemic control, insulin sensitivity, and beta-cell function in type 2 diabetes: a parallel-group study. *Lancet* **359**, 824–830.

### Acknowledgements

We thank the Wellcome Trust and Diabetes UK for their support. F.M.G. is a Wellcome Trust Senior Research Fellow in Clinical Science, F.R. is a Diabetes UK R. D. Lawrence Fellow. This work was supported in part by an operating grant from the Canadian Institutes for Health Research and a Canada Research Chair in Regulatory Peptides (D.J.D.). We thank X. Cao for expert help with the PCR experiments.

### Supplementary material

The online version of this paper can be accessed at:

DOI: 10.1113/jphysiol.2004.076414

[http://jp.physoc.org/cgi/content/full/jphysiol.](http://jp.physoc.org/cgi/content/full/jphysiol.2004.076414/DC1)

[2004.076414/DC1](http://jp.physoc.org/cgi/content/full/jphysiol.2004.076414/DC1)

and contains supplementary material containing sequences of primers and specific conditions used for RT-PCR experiments.

This material can also be found at:

<http://www.blackwellpublishing.com/products/journals/suppmat/tjp/tjp705/tjp705sm.htm>